

# Combined Convection in a Lid-Driven Cavity with an Inside Obstacle Subjected to $\text{Al}_2\text{O}_3$ -Water Nanofluid: Effect of Solid Volume Fraction and Nanofluid Variable Properties

M. HEMMAT ESFE<sup>a,\*</sup>, A. ZARE GHADI<sup>b</sup>, S.S. MIRTALEBI ESFORJANI<sup>a</sup> AND M. AKBARI<sup>a</sup>

<sup>a</sup>Department of Mechanical Engineering, Najafabad Branch, Islamic Azad University, Isfahan, Iran

<sup>b</sup>Department of Mechanical Engineering, Jouybar Branch, Islamic Azad University, Jouybar, Iran

(Received January 3, 2013; in final form May 17, 2013)

The phenomena of combined convection within a lid-driven square cavity subjected to variable properties of nanofluid having a hot obstacle have been analyzed numerically. Finite volume method with SIMPLER algorithm is employed for solving the Navier–Stokes and energy balance equations. In this paper diameter of nanoparticles are uniform, constant and equal to 47 nm. Wide range of parameters such as Richardson number ( $0.01 < \text{Ri} < 100$ ), solid volume fraction ( $0.00 < \varphi < 0.05$ ), temperature of fluid ( $300 < T < 340$ ) and height of heated obstacle ( $0.1 < h < 0.3$ ) have been used. Numerical results are presented in terms of streamlines, isotherms and average Nusselt numbers diagram. The comparisons show that the average Nusselt number decreases with increasing temperature of nanofluid for the whole range of the Richardson numbers. Also heat transfer augments as the height of heat obstacle on the bottom wall increases.

DOI: [10.12693/APhysPolA.124.665](https://doi.org/10.12693/APhysPolA.124.665)

PACS: 47.11.-j, 47.11.Df, 47.15.Rq, 47.55.pb, 47.61.-k

## 1. Introduction

Nanofluid, which is a mixture of nano-sized particles dispersed in a pure fluid, has a higher thermal conductivity than the pure fluid. This higher thermal conductivity enhances rate of heat transfer in this fluid. In recent decades, many researchers have investigated different aspects of nanofluids (Godson et al. [1]).

Mixed convection is a type of convection which consists of both natural and forced convection. The interaction of buoyancy force and shear force makes mixed convection heat transfer a complex concept. Numerous investigations have been conducted on the mixed convection heat transfer in cavities filled with nanofluids. Khanafer and Chamkha [2] carried out a numerical study on mixed convection flow in a lid-driven enclosure subjected to a fluid-saturated porous medium. Aydin [3] performed the study of opposing and aiding mechanisms of mixed convection in a shear and buoyancy driven cavity. Chamkha [4] continued the Aydin study [3] and numerically investigated hydromagnetic mixed convection flow in a vertical lid-driven cavity with internal heat absorption or generation. The result showed that for constant Grashof number, increasing the Reynolds number causes enhancement of heat transfer rate. In another study, Khanafer et al. [5] executed a study on unsteady mixed convection in a lid-driven enclosure utilizing an externally excited sliding lid. Tiwari et al. [6] investigated flow and heat transfer in a square cavity with insulated top and bottom

walls and differentially-heated moving side walls using the finite volume method. The cavity was filled with the copper–water nanofluid. Conducting a parametric study, they studied impact of the Richardson number and volume fraction of the nanoparticles on the heat transfer inside the cavity and observed that for the Richardson number equal to unity the average Nusselt number increased substantially with increase in the volume fraction of the nanoparticles. In another study, Ho et al. [7] studied influences of uncertainties due to adapting different models for the effective thermal conductivity and the dynamic viscosity of alumina–water nanofluid on the natural convection heat transfer in a square enclosure. Their findings indicated that the heat transfer across the cavity could be either enhanced or mitigated with respect to that of the base fluid depending on the model used for the thermal conductivity and the viscosity of the nanofluid.

Muthtamilselvan et al. [8] made a numerical investigation of the mixed convection flow and heat transfer of copper–water nanofluid in a lid-driven cavity for different aspect ratios using the control volume method. The left and right walls were insulated while the top and bottom walls were kept at constant temperatures, with the top wall moving at a constant velocity. They observed that both the aspect ratio of the cavity as well as the nanoparticles volume fraction affected the fluid flow and heat transfer inside the enclosure. Study on mixed convection flows in a lid-driven enclosure utilizing Cu–water nanofluid was carried out numerically by Talebi et al. [9] employing the finite volume method.

The vertical walls of the cavity were differentially heated while its top and bottom walls were kept insulated. Their results showed that for specified Reynolds

\*corresponding author; e-mail: [M.hemmatesfe@gmail.com](mailto:M.hemmatesfe@gmail.com)

and Rayleigh numbers, increase in the volume fraction of the nanoparticles enhanced the heat transfer inside the enclosure. Results of a numerical study on mixed convection in a lid-driven nanofluid filled square cavity with cold side and top wall and a constant heat flux heater on the bottom wall and moving lid were reported by Mansoor et al. [10]. The impact of the Reynolds number, type of nanofluids, size and location of the heater and the volume fraction of the nanoparticles were considered in their investigation. Their results indicate that the rate of heat transfer enhanced with increase in the length of the heater, the Reynolds number, and the nanoparticles volume fraction.

The problem of mixed convection in a ventilated, partially heated from below square cavity was studied numerically by Shahi et al. [11]. The cavity had an inlet and outlet in lower corner of left wall and upper corner of right wall, respectively, and a constant heat flux heater on the middle of the bottom wall. Abu-Nada and Chamkha [12] studied numerically mixed convection in a nanofluid-filled inclined square cavity. Their results showed that the presence of nanoparticles enhanced the heat transfer inside the cavity significantly.

Ghasemi and Aminossadati [13] investigated mixed convection of  $\text{Al}_2\text{O}_3$ -water nanofluid inside a right triangular cavity with insulated horizontal wall, hot inclined wall, and moving cold vertical wall. They considered effects of the Richardson number, nanoparticles volume fraction and two different upward and downward movement of the cold vertical wall. Their results showed that addition of the nanoparticles enhanced the rate of heat transfer for all values of the Richardson number and for each direction of the sliding wall motion.

Mahmoodi [14] conducted a numerical study to examine the mixed convection flow inside rectangular cavities subjected to  $\text{Al}_2\text{O}_3$ -water nanofluid with moving bottom wall and cold top, left and right walls. He observed significant enhancement in the heat transfer rate in the cavity due to the existence of the nanoparticles for all values of the Richardson number considered. Very recently Arefmanesh and Mahmoodi [15] performed a numerical study to examine effects of uncertainties of viscosity models for the  $\text{Al}_2\text{O}_3$ -water nanofluid on mixed convection in a square cavity with cold left, right, and top walls and moving hot bottom wall. They used two different viscosity models and found that significant differences existed between the magnitudes of heat transfer enhancement for the two viscosity models employed.

Sebdani et al. [16] conducted a numerical study to examine the effect of nanofluid variable properties on mixed convection in a square enclosure with moving right and left walls and a constant temperature heater on the bottom wall. They found that in different Reynolds and Rayleigh numbers, the heat transfer of the nanofluid could be either enhanced or mitigated with respect to that of the pure fluid. Influence of using nanofluid on mixed convection flow and heat transfer in an inclined double lid-driven cavity having two heated obstacles has

been performed by Hemmat Esfe et al. [17]. In their investigation, the effect of the Rayleigh number, solid volume fraction of nanoparticle, height of heated obstacle, and cavity inclination angles are analyzed and discussed.

The present paper will focus on effects of temperature and solid volume fraction dependent thermal conductivity and viscosity models on mixed convection of nanofluid in a lid-driven cavity containing a heated obstacle subjected to nanofluid. The  $\text{Al}_2\text{O}_3$ -water nanofluid is employed in this way. The correlation derived by Jang et al. [18] and Xu et al. [19] based on the detailed experimental results will be used for nanofluids viscosity and thermal conductivity, respectively.

## 2. Physical modeling and governing equations

A schematic view of the lid-driven cavity subjected to a nanofluid considered in the present paper is displayed in Fig. 1. The height and the width of the square cavity are denoted by  $L$ . The bottom and vertical walls are kept insulated whereas the top moving wall is maintained at low temperature ( $T_c$ ). An obstacle with a relatively higher temperature ( $T_h$ ) is located on the bottom wall of the cavity. The length and the height of the hot obstacle are denoted by  $d$  and  $h$ , respectively.

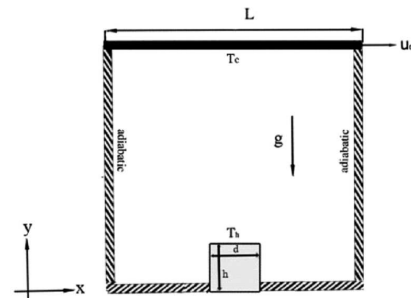


Fig. 1. Schematic view of current study.

TABLE I

Thermophysical properties of water and nanoparticles at  $T = 25^\circ\text{C}$ .

Physical properties	Fluid phase (water)	Solid ( $\text{Al}_2\text{O}_3$ )
$C_p$ [J/(kg K)]	4179	765
$\rho$ [ $\text{kg}/\text{m}^3$ ]	997.1	3970
$K$ [ $\text{W m}^{-1} \text{K}^{-1}$ ]	0.6	25
$\beta \times 10^{-5}$ [1/K]	21.0	0.85
$\mu \times 10^{-4}$ [kg/m]	8.9	–
$d_p$ [nm]	0.384	47

The nanofluid in the cavity is Newtonian, incompressible and laminar. In addition, it is assumed that both the fluid phase and nanoparticles are in the thermal equilibrium state and they flow with the same velocity. The density variation in the body force term of the momentum equation is satisfied by Boussinesq's approximation.

The thermophysical properties of nanoparticles and the water as the base fluid at  $T = 25^\circ\text{C}$  are presented in Table I.

The thermal conductivity and the viscosity of the nanofluid are taken into consideration as variable properties; both of them change with volume fraction and temperature of nanoparticles. Under the above assumptions, the system of governing equations is

$$\frac{\partial u}{\partial x} + \frac{\partial v}{\partial y} = 0, \quad (1)$$

$$u \frac{\partial u}{\partial x} + v \frac{\partial u}{\partial y} = -\frac{1}{\rho_{\text{nf}}} \frac{\partial p}{\partial x} + \nu_{\text{nf}} \nabla^2 u, \quad (2)$$

$$u \frac{\partial v}{\partial x} + v \frac{\partial v}{\partial y} = -\frac{1}{\rho_{\text{nf}}} \frac{\partial p}{\partial y} + \nu_{\text{nf}} \nabla^2 v + \frac{(\rho\beta)_{\text{nf}}}{\rho_{\text{nf}}} g \Delta T, \quad (3)$$

and

$$u \frac{\partial T}{\partial x} + v \frac{\partial T}{\partial y} = \alpha_{\text{nf}} \nabla^2 T. \quad (4)$$

The dimensionless parameters may be presented as

$$X = \frac{x}{L}, \quad Y = \frac{y}{L}, \quad V = \frac{v}{u_0}, \quad U = \frac{u}{u_0},$$

$$\Delta T = T_h - T_c, \quad \theta = \frac{T - T_c}{\Delta T}, \quad P = \frac{p}{\rho_{\text{nf}} u_0^2}. \quad (5)$$

Hence,

$$\text{Re} = \frac{\rho_f u_0 L}{\mu_f}, \quad \text{Ri} = \frac{\text{Ra}}{\text{Pr Re}^2}, \quad \text{Ra} = \frac{g \beta_f \Delta T L^3}{\nu_f \alpha_f},$$

$$\text{Pr} = \frac{\nu_f}{\alpha_f}. \quad (6)$$

The dimensionless form of the above governing Eqs. (1) to (4) become

$$\frac{\partial U}{\partial X} + \frac{\partial V}{\partial Y} = 0, \quad (7)$$

$$U \frac{\partial U}{\partial X} + V \frac{\partial U}{\partial Y} = -\frac{\partial P}{\partial X} + \frac{\nu_{\text{nf}}}{\nu_f} \frac{1}{\text{Re}} \nabla^2 U, \quad (8)$$

$$U \frac{\partial V}{\partial X} + V \frac{\partial V}{\partial Y} = -\frac{\partial P}{\partial Y} + \frac{\nu_{\text{nf}}}{\nu_f} \frac{1}{\text{Re}} \nabla^2 V + \frac{\text{Ri}}{\text{Pr}} \frac{\beta_{\text{nf}}}{\beta_f} \Delta \theta, \quad (9)$$

and

$$U \frac{\partial \theta}{\partial X} + V \frac{\partial \theta}{\partial Y} = \frac{\alpha_{\text{nf}}}{\alpha_f} \nabla^2 \theta. \quad (10)$$

### 2.1. Thermal diffusivity and effective density

Thermal diffusivity and effective density of the nanofluid are

$$\alpha_{\text{nf}} = \frac{k_{\text{nf}}}{(\rho c_p)_{\text{nf}}}, \quad (11)$$

$$\rho_{\text{nf}} = \varphi \rho_s + (1 - \varphi) \rho_f. \quad (12)$$

### 2.2. Heat capacity and thermal expansion coefficient

Heat capacity and thermal expansion coefficient of the nanofluid are therefore

$$(\rho c_p)_{\text{nf}} = \varphi (\rho c_p)_s + (1 - \varphi) (\rho c_p)_f, \quad (13)$$

$$(\rho \beta)_{\text{nf}} = \varphi (\rho \beta)_s + (1 - \varphi) (\rho \beta)_f. \quad (14)$$

### 2.3. Viscosity

The effective viscosity of nanofluid was calculated by

$$\mu_{\text{eff}} = \mu_f (1 + 2.5\varphi) \left[ 1 + \eta \left( \frac{d_p}{L} \right)^{-2\varepsilon} \varphi^{2/3} (\varepsilon + 1) \right]. \quad (15)$$

This well-validated model is presented by Jang et al. [18] for a fluid containing a dilute suspension of small rigid spherical particles and it accounts for the slip mechanism in nanofluids. The empirical constant  $\varepsilon$  and  $\eta$  are 0.25 and 280 for  $\text{Al}_2\text{O}_3$ , respectively.

It is worth mentioning that the viscosity of the base fluid (water) is considered to vary with temperature and the flowing equation is used to evaluate the viscosity of water,

$$\mu_{\text{H}_2\text{O}} = (1.2723T_{\text{rc}}^5 - 8.736T_{\text{rc}}^4 + 33.708T_{\text{rc}}^3 - 246.6T_{\text{rc}}^2 + 518.78T_{\text{rc}} + 1153.9) \times 10^6, \quad (16)$$

where

$$T_{\text{rc}} = \log(T - 273).$$

### 2.4. Dimensionless stagnant thermal conductivity

The effective thermal conductivity of the nanoparticles in the liquid as stationary is calculated by the Hamilton and Crosser (H-C model [20]), which is

$$\frac{k_{\text{stationary}}}{k_f} = \frac{k_s + 2k_f - 2\varphi(k_f - k_s)}{k_s + 2k_f + \varphi(k_f - k_s)}. \quad (17)$$

### 2.5. Total dimensionless thermal conductivity of nanofluids

Total dimensionless thermal conductivity of nanofluids is

$$\frac{k_{\text{nf}}}{k_f} = \frac{k_{\text{stationary}}}{k_f} + \frac{k_c}{k_f} = \frac{k_s + 2k_f - 2\varphi(k_f - k_s)}{k_s + 2k_f + \varphi(k_f - k_s)} + c \frac{\text{Nu}_p d_f (2 - D_f) D_f \left[ \left( \frac{d_{\text{max}}}{d_{\text{min}}} \right)^{1-D_f} - 1 \right]^2}{\text{Pr}(1 - D_f)^2 \left( \frac{d_{\text{max}}}{d_{\text{min}}} \right)^{2-D_f} - 1} \frac{1}{d_p}. \quad (18)$$

This model was proposed by Xu et al. [19] and it has been chosen in this study to describe the thermal conductivity of nanofluids.  $c$  is an empirical constant (e.g.  $c = 85$  for the deionized water and  $c = 280$  for ethylene glycol) but independent of the type of nanoparticles.  $\text{Nu}_p$  is the Nusselt number for liquid flowing around a spherical particle and equal to two for a single particle in this work. The fluid molecular diameter  $d_f = 4.5 \times 10^{-10}$  m for water in present study. The fractal dimension  $D_f$  is determined by

$$D_f = 2 - \frac{\ln \varphi}{\ln \left( \frac{d_{p,\text{min}}}{d_{p,\text{max}}} \right)}$$

where  $d_{p,\text{max}}$  and  $d_{p,\text{min}}$  are the maximum and minimum diameters of nanoparticles, respectively. Ratio of minimum to maximum nanoparticles  $d_{p,\text{min}}/d_{p,\text{max}}$  is  $R$ .

In this investigation  $R$  is constant and equal to 0.007:

$$d_{p,\max} = d_p \frac{D_f - 1}{D_f} \left( \frac{d_{p,\min}}{d_{p,\max}} \right)^{-1},$$

$$d_{p,\min} = d_p \frac{D_f - 1}{D_f}.$$

### 3. Numerical method

Governing equations for continuity, momentum and energy equations associated with the boundary conditions in this investigation were calculated numerically based on the finite volume method and associated staggered grid system, using FORTRAN computer code. The SIMPLE algorithm is used to solve the coupled system of governing equations. The convection term is approximated by a hybrid-scheme which is conducive to a stable solution. In addition, a second-order central differencing scheme is utilized for the diffusion terms. The resulting discretized equations are solved iteratively by Tri-diagonal matrix algorithm (TDMA) in a line going through all volumes in the computational domain. The iteration process is terminated when the following condition is satisfied:

$$\left| \frac{\sum (\phi_{i,j}^t - \phi_{i,j}^{t-1})}{\sum \phi_{i,j}^t} \right| \leq 10^{-6},$$

where  $\phi$  refers to  $\theta$ ,  $U$ , and  $V$ , and  $t$  indicates the iteration step.

To verify grid independence, numerical procedure was carried out for nine different mesh sizes. Average Nu of the hot wall at  $w = 0.2$ ,  $h = 0.2$ ,  $\phi = 0.01$  and different

Richardson numbers, is obtained for each grid size as shown in Fig. 2.

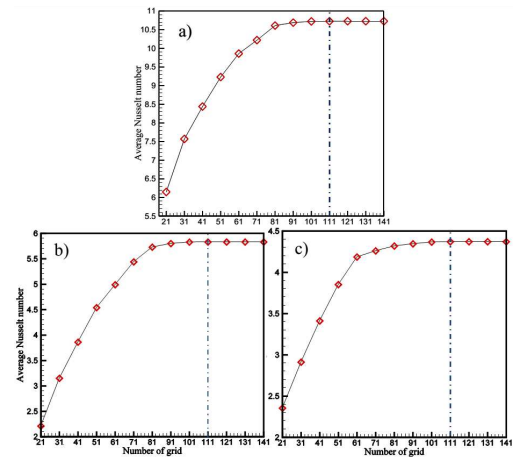


Fig. 2. Mesh validation for different Richardson numbers: (a)  $Ri = 0.1$ , (b)  $Ri = 10$ , (c)  $Ri = 100$ .

As can be observed, an  $111 \times 111$  uniform grid size yields the required accuracy for different Richardson numbers and was hence applied for all simulation exercises in this work as presented in the following section.

To ensure the accuracy and validity of this new model, we analyze a square cavity filled with base fluid and different  $Re$  and  $Ri$  numbers. Table II shows the comparison between the results obtained with the current study and the values presented in the literature. The quantitative comparisons for the average Nusselt numbers indicate an excellent agreement between them.

Comparison between the results in present study and other researches.

TABLE II

Re	Ri	Present study	Abu-Nada et al. [12]	Waheed [24]	Tiwari and Das [6]	Abdelkhalek [23]	Khanafer et al. [5]	Sharif [22]	Khanafer and Chamkha [2]	Iwatsu et al. [21]
1	100	0.991	1.01	1.000	–	–	–	–	–	–
100	0.01	2.016	2.09	2.031	2.10	1.985	2.020	–	2.010	1.940
400	0.0006	3.9	4.162	4.024	3.85	3.878	4.01	4.05	3.91	3.84
500	0.0004	4.476	4.663	4.526	–	–	–	–	–	–
1000	0.0001	6.39	6.551	6.484	6.33	6.345	6.42	6.55	6.33	6.33

Also the proposed numerical scheme was validated by using the numerical results published by Lin and Violi [25] in Fig. 3.

Finally, for validating flow patterns and streamlines, conditions of physical domain of present code was mimicked with the conditions as invoked by Talebi et al. [9] and also Iwatsu et al. [21]. Figures 4 and 5 show agreement between present code (right one) and the literature (left one).

In order to evaluate Xu’s model, Fig. 6 indicates the characteristic of the effective thermal conductivity, which

is a function of the practical parameters  $T$ ,  $d_p$  and  $R = d_{p,\min}/d_{p,\max}$ . As presented in this figure,  $R$  has significant effect for small average nanoparticle diameters.

### 4. Results and discussion

In this paper, square cavity filled with water–aluminum oxide nanofluid with moving upper lid and four-sided hot obstacle was numerically simulated. The influence of parameters such as hot obstacle height in the cavity, nanofluid temperature, nanofluid solid volume

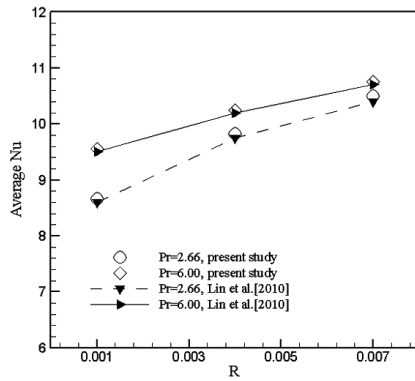


Fig. 3. Comparison of average Nusselt numbers between Lin et al. and the present result for  $Gr = 10^5$ ,  $d_p = 5$  nm, and  $\varphi = 0.05$  for different values of Pr numbers.

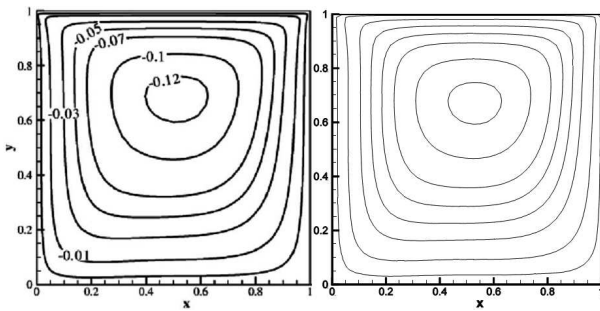


Fig. 4. Comparison of streamlines between result of Talebi et al. [9] (left) and present code (right).

fraction and Richardson number have been investigated on fluid flow and its thermal behavior.

Figure 7 displays streamline and temperature field for different nanofluid solid volume fractions inside the cavity in  $T = 300$ ,  $d_p = 47$  nm,  $Ri = 0.01$ ,  $h = 0.1L$ . The flow pattern displays a central clockwise cell with circular nucleus which occupies vast part of cavity internal space. The formation of this cell results from the reaction of shear force caused by upper lid movement and buoyancy force caused by temperature difference inside

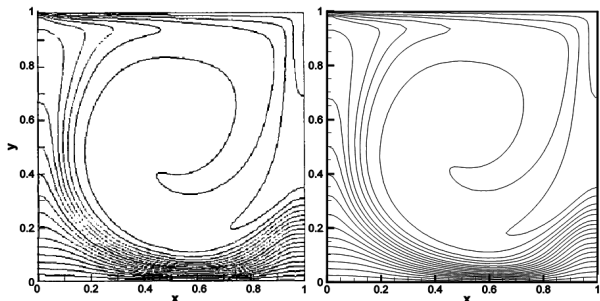


Fig. 5. Comparison of isotherms between result of Iwatsu et al. [21] (left) and present code (right).

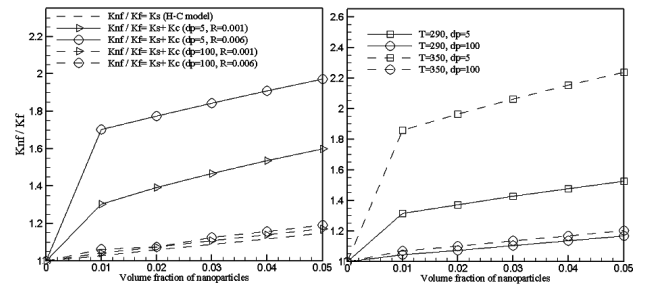


Fig. 6. Dimensionless effective thermal conductivity of  $Al_2O_3$  - water nanofluid versus concentration of nanoparticles with different mean nanoparticle diameters and fractal distributions: (a)  $T = 300$  and (b)  $R = 0.004$ .

the cavity. In the geometry under investigation in this paper, shear and buoyancy forces act in the same direction and resonate each other while forming a central cell. Also, two small vortices were formed on the sides of the obstacle that the right side vortex is slightly stronger. Paying close attention to figure corresponding to streamlines, one could infer that addition of nanofluid to base fluid causes reduction in severity and velocity of central cell inside the cavity.

Also increasing solid volume fraction reduces intensity of the central cell. Temperature lines are highly intense in areas close to hot walls that such intensity and temperature gradient decrease through increasing solid volume fraction. Primary reason for temperature gradient reduction with increasing solid volume fraction is an increase in nanofluid thermal conductivity compared to the base fluid. It is not possible to comment on cavity general thermal conductivity in this state, because reduction in temperature gradient accompanies increase in thermal conductivity coefficient, and heat transfer inside the cavity depends upon these two parameters.

Figure 8 displays changes in fluid flow and its thermal distribution at different heights of hot obstacle inside the cavity in  $Ri = 100$ ,  $\varphi = 0.05$ ,  $T = 300$  K and  $d_p = 47$  nm. In this state, flow pattern displays a strong central cell with an oval nucleus in the center of the cavity which has almost occupied the entire cell space. With increasing the height of the obstacle, the intensity of clockwise central cell reduces and central core loses its symmetrical circular shape and accommodates oval shape. Additionally, isotherm lines separate slightly from each other near isotherm walls with increasing obstacle height, and temperature gradient decreases with increasing obstacle height. It is therefore expected that decreasing temperature gradient results in average Nusselt number reduction and heat transfer in the cavity.

The effects of temperature on streamlines and nanofluid thermal behavior are displayed in Fig. 9. As a result of employing new models of variable characteristics to estimate viscosity and thermal conductivity coefficient in this study, the temperature and diameter of nanopar-

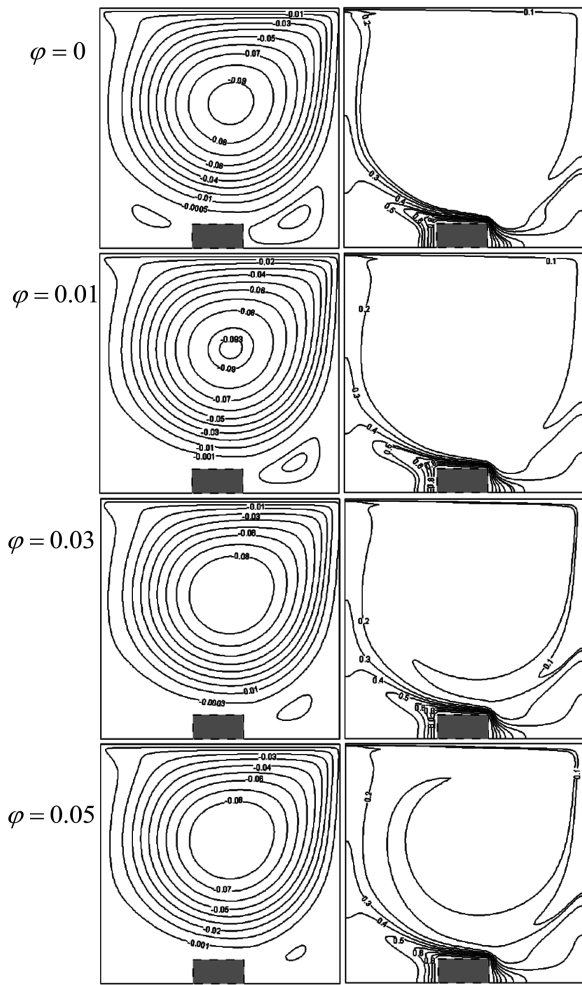


Fig. 7. Streamlines and isotherm for different solid volume fraction of nanofluid at  $T = 300$ ,  $d_p = 47$  nm,  $Ri = 0.01$ ,  $h = 0.1L$ .

ticles, too, have influence on heat transfer and fluid flow in the cavity. Investigating these effects is among the novelties of the present study. These analyses, despite their applied importance, have not been attended to inclusively by research groups. As it is evident in these figures, with increasing temperature, streamlines intensify in central cell and severity and velocity of clockwise central cell increases. Increasing severity and velocity of central cell causes relative reduction of isotherm lines and as a result temperature gradient reduction near hot walls. Accordingly, it could be expected that regarding temperature gradient reduction with increasing nanofluid temperature, heat transfer inside the cavity slightly decreases as well.

Figure 10 shows the Nusselt number changes on the basis of the Richardson number for obstacle different heights in  $\varphi = 0.05$ ,  $d_p = 47$  nm and  $T = 300$ . As it was expected and was already stated when analyzing isotherm lines, increasing hot obstacle height causes reduction in the Nusselt number and hence heat transfer.

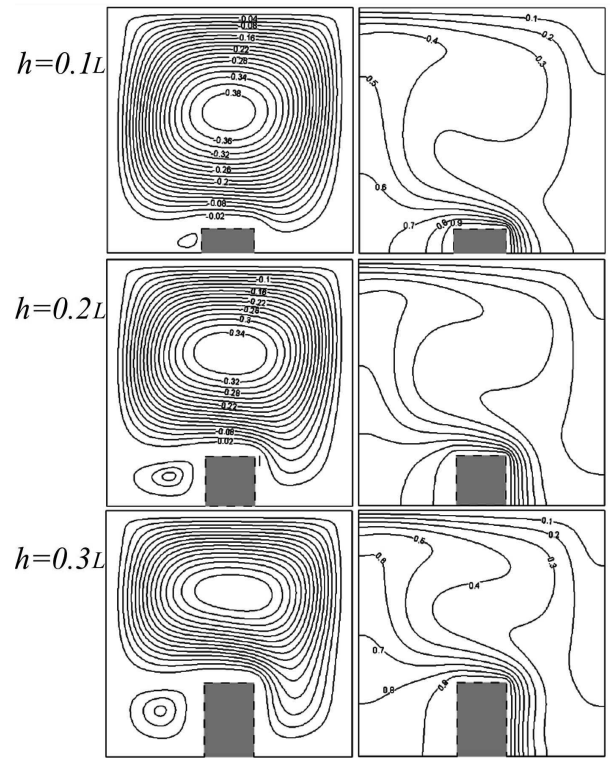


Fig. 8. Streamlines and isotherm for different height of heated obstacle at  $Ri = 100$ ,  $\varphi = 0.05$ ,  $T = 300$  K and  $d_p = 47$  nm.

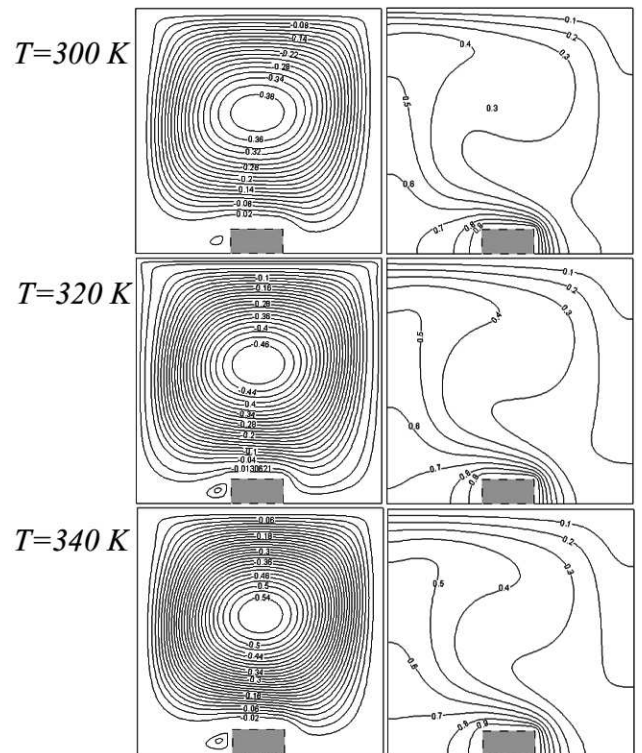


Fig. 9. Streamlines and isotherm for different temperature of nanofluid at  $Ri = 100$ ,  $\varphi = 0.05$ ,  $h = 0.1L$  and  $d_p = 47$  nm.

Increasing the Richardson number at all heights results in reduction of the Nusselt number and such reduction is resulting by dominance of buoyancy compared to shear force and dominance of natural moving force over forced moving one. Also, in higher Richardson values, changes in obstacle height causes more difference in heat transfer and Nusselt number.

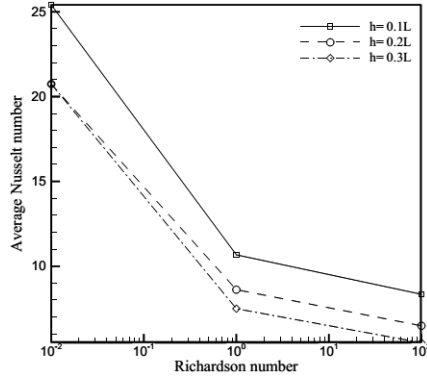


Fig. 10. Average Nusselt number versus Richardson number for different heights of hot obstacle at  $d_p = 47$  nm,  $\varphi = 0.05$ , and  $T = 300$  K.

Figure 11 displays the Nusselt number changes with respect to the Richardson number for different temperatures in  $\varphi = 0.05$ ,  $h = 0.1L$  and  $d_p = 47$  nm. As it was predicted, increase in the temperature of the nanofluid causes in reduction of the Nusselt number and heat transfer in the cavity and such Nusselt number reduction is more at higher Richardson values.

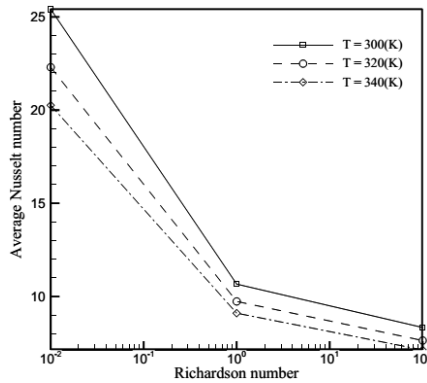


Fig. 11. Average Nusselt number versus Richardson number for different temperatures at  $\varphi = 0.05$ ,  $h = 0.1L$  and  $d_p = 47$  nm.

Reduction in heat transfer from the height of 0.1 to 0.3 of side length equals 26.16% in 0.01 Richardson and 18.28% in Richardson of unity and 15.6% in Richardson of 100. As the percentage of the Nusselt number reduction indicates, percentage reduction decreases with increasing Richardson value. In addition, identical to the previous diagram, heat transfer reduces in the cavity with increasing Richardson number that is caused by forced movement reduced against natural movement.

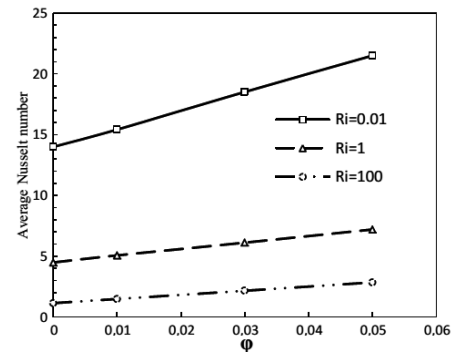


Fig. 12. Average Nusselt number versus solid volume fraction for Richardson numbers at  $T = 300$  K,  $h = 0.2L$  and  $d_p = 47$  nm.

Figure 12 indicates average Nusselt number versus solid volume fraction. The increase of the solid concentration amplifies the effective thermal conductivity and hence the energy transfer. The increase of the solid concentration also increases the flow intensity. Both of two factors increase the average Nusselt number with solid concentration. Moreover, for a fixed value of volume fraction of nanoparticles, the average Nusselt number increases as the Richardson number decreases. The Richardson number decreases with increase in the Reynolds number when the Grashof number is kept constant. Consequently, by augmentation in the Richardson number (the Reynolds number decreases) the forced convection becomes weaker; that is why the rate of heat transfer increases.

## 5. Conclusion

In this study, the problem of mixed convection lid-driven cavity subjected to variable properties of nanofluid ( $\text{Al}_2\text{O}_3$ -water) with an inside hot obstacle was performed numerically. A parametric study was done and effects of the volume fraction of the  $\text{Al}_2\text{O}_3$  nanoparticles, height of hot obstacle and temperature of nanofluid on the heat transfer performance inside the cavity were studied and the following results were obtained:

1. For all considered cases, when the volume fraction of the nanoparticles and the Richardson number are kept constant, the rate of heat transfer decreases by increase of the temperature of nanofluid.
2. Increasing height of the cavity reduces the temperature gradient around hot walls and consequently decreases average Nusselt number.
3. When the temperature and height of hot obstacle are kept constant, the average Nusselt number increases by decrease in the Richardson number.

## References

- [1] L. Godson, B. Raja, D.M. Lal, S. Wongwises, *Renew. Sustain. En. Rev.* **14**, 629 (2010).
- [2] K. Khanafer, A.J. Chamkha, *Int. J. Heat Mass Transf.* **42**, 2465 (1999).
- [3] O. Aydin, *Int. Commun. Heat Mass Transf.* **26**, 1019 (1999).

- [4] A.J. Chamkha, *Num. Heat Transf., Part A* **41**, 529 (2002).
- [5] K.M. Khanafar, A.M. Al-Amiri, I. Pop, *Europ. J. Mech. B/Fluids* **26**, 669 (2007).
- [6] R.K. Tiwari, M.K. Das, *Int. J. Heat Mass Transf.* **50**, 2002 (2007).
- [7] C.J. Ho, M.W. Chen, Z.W. Li, *Int. J. Heat Mass Transf.* **51**, 4506 (2008).
- [8] M. Muthtamilselvan, P. Kaswamy, J. Lee, *Commun. Nonlinear Sci. Numer. Simulat.* **15**, 1501 (2010).
- [9] F. Talebi, A.H. Mahmoudi, M. Shahi, *Int. Commun. Heat Mass Transf.* **37**, 79 (2010).
- [10] M.A. Mansour, R.A. Mohamed, M.M. Abd-Elaziz, S.E. Ahmed, *Int. Commun. Heat Mass Transf.* **37**, 1504 (2010).
- [11] M. Shahi, A.H. Mahmoudi, F. Talebi, *Int. Commun. Heat Mass Transf.* **37**, 201 (2010).
- [12] E. Abu-Nada, A.J. Chamkha, *Europ. J. Mech. B/Fluids* **29**, 472 (2010).
- [13] B. Ghasemi, S.M. Aminossadati, *Int. Commun. Heat Mass Transf.* **37**, 1142 (2010).
- [14] M. Mahmoudi, *Therm. Sci.* **15**, 889 (2011).
- [15] A. Arefmanesh, M. Mahmoudi, *Int. J. Therm. Sci.* **50**, 1706 (2011).
- [16] S. Mazrouei Sebdani, M. Mahmoudi, S.M. Hashemi, *Int. J. Therm. Sci.* **52**, 112 (2012).
- [17] M. Hemmat Esfe, A. Haghiri, M. Rabbani Bidgoli, S.A. Hosseini, .
- [18] S.P. Jang, J.H. Lee, K.S. Hwang, S.U.S. Choi, *Appl. Phys. Lett.* **91**, 24 (2007).
- [19] J. Xu, B. Yu, M. Zou, P. Xu, *J. Phys. D* **39**, 4486 (2006).
- [20] R.L. Hamilton, O.K. Crosser, *Indust. Eng. Chem. Fund.* **1**, 187 (1962).
- [21] R. Iwatsu, J. Hyun, K. Kuwahara, *Int. J. Heat Mass Transf.* **36**, 1601 (1993).
- [22] M.A.R. Sharif, *Appl. Therm. Eng.* **27**, 1036 (2007).
- [23] M.M. Abdelkhalek, *Comput. Mater. Sci.* **42**, 212 (2008).
- [24] M.A. Waheed, *Int. J. Heat Mass Transf.* **52**, 5055 (2009).
- [25] K.C. Lin, A. Violi, *Int. J. Heat Fluid Flow* **31**, 236 (2010).